Kelvin Fronts on the Equatorial Thermocline

ALEXEY V. FEDOROV

Atmospheric and Oceanic Sciences, Princeton University, Princeton, New Jersey

W. KENDALL MELVILLE

Scripps Institution of Oceanography, University of California, San Diego, La Jolla, California

ABSTRACT

Properties of internal wave fronts or Kelvin fronts travelling eastward in the equatorial waveguide are studied, motivated by recent studies on coastal Kelvin waves and jumps and new data on equatorial Kelvin waves. It has been recognized for some time that nonlinear equatorial Kelvin waves can steepen and break, forming a broken wave of depression, or front, propagating eastward. The three-dimensional structure of the wave field associated with such a front is considered. As for linear Kelvin waves, the front is symmetrical with respect to the equator. Sufficiently far away from the front, the wave profile is Gaussian in the meridional direction, with the equatorial Rossby radius of deformation being its decay scale. Due to nonlinearity, the phase speed of the front is greater than that of linear Kelvin waves, resulting in a supercritical flow. This leads to the resonant generation of equatorially trapped gravity–inertial (or Poincaré) waves, analogous in principle to the resonant mechanism for nonlinear coastal Kelvin waves. First-mode symmetrical Poincaré waves are generated, with their wavelength determined by the amplitude of the front. Finally, the propagation of a Kelvin front gives rise to a nonzero poleward mass transport above the thermocline, in consequence of which there is a poleward heat flux.

1. Introduction

The propagation of internal Kelvin waves on the equatorial thermocline plays an important role in equatorial dynamics. Figure 1 [Tropical Atmosphere–Ocean (TAO) array data] shows that the equatorial ocean can be well-described within the framework of a two-layer model. The Coriolis parameter vanishes at the equator so that the interface between the shallow and the deep layer serves as a waveguide for various trapped waves, including eastward travelling Kelvin waves and westward travelling Rossby waves. Trapped gravity–inertial waves (or Poincaré waves) can propagate in both directions, although the first gravity–inertial wave mode has properties of a Rossby wave when it travels westward [mixed Rossby–gravity or Yanai wave, Gill (1982); see Fig. 6 below].

Boyd (1980) and Ripa (1982) considered nonlinear equatorial Kelvin waves and showed that they could steepen and overturn or break. A wave of depression deepens the thermocline and breaks on the forward face of the wave, while a wave of elevation raises the ther-mocline and tends to break on the rearward face. A broken wave of depression can form a jump [also called shocks or fronts: Lighthill (1978), Philander (1990)]. In this paper we propose a model for such fronts (we call them equatorial Kelvin fronts) and study the properties. Earlier, Fedorov and Melville (1995, 1996) and Fedorov (1997) studied properties of nonlinear Kelvin waves and fronts trapped near coastal boundaries; this work considers analogous phenomena in the equatorial ocean. Whether Kelvin waves are linear waves or nonlinear fronts determines their main characteristics, including the speed of wave propagation, dissipation rates, and the meridional structure of the flow.

Extensive data on Kelvin waves have been obtained recently, motivated in part by possible connection between the initial stages of El Niño and equatorial Kelvin waves which may precede this event: Any relaxation or reversal of the steady trade winds (the easterlies) results in the excitation of a Kelvin wave, which can affect El Niño (e.g., Federov 2000, Manuscript in preparation). The periods of equatorial Kelvin waves vary from two weeks (Philander 1984) to two months (Kessler et al. 1995) and even to intraseasonal timescales [up to four months: Johnson and McPhaden (1993)]. The motion is characterized by zero flux across the equator. The typical phase speed of the waves ranges from 2 to 3 m s^{-1} and depends upon the depth of the thermocline and nonlinear effects.

Corresponding author address: Alexey Fedorov, Program in Atmospheric and Oceanic Sciences, Princeton University, P.O. Box CN710, Sayre Hall, Princeton, NJ 08544-0710.
E-mail: alexey@princeton.edu

MONTHLY MEAN TAO TEMPERATURES (°C)
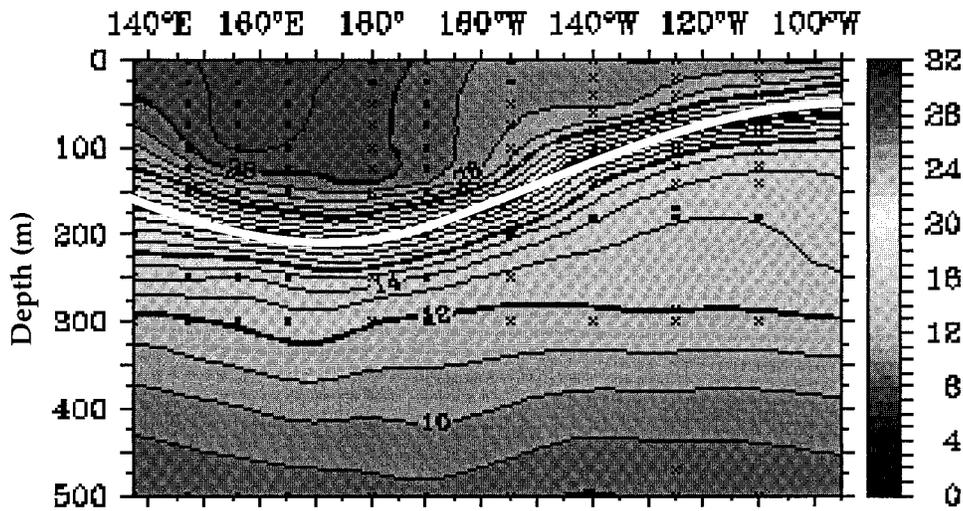### MARCH 1997; 2° S to 2° N Average

Fig. 1. Temperature distribution in the Pacific Ocean at the equator in Mar 1997. The thermocline corresponds to about 20°C (from the TAO Web site). Note the almost vertical 27°–28°C isotherms around 180° indicating the possibility of front formation.

Are nonlinear effects important for equatorial Kelvin waves? Delcroix et al. (1991) studied equatorial Kelvin waves in the Pacific ocean through Geosat measurements of sea level and surface current anomalies. The measured phase speed of the waves was 2.82 ± 0.96 m s^{-1}, while theoretical predictions of the linear phase speed were in the range 2.26 ± 1.02 m s^{-1}. Kessler et al. (1995) looked at the displacement of the thermocline during passages of Kelvin waves and found amplitudes $a = \pm 20$ m, with the depth of the thermocline varying from 80 to 170 m. Eriksen et al. (1983) measured sea-level fluctuations of about 10 cm, which they attributed to signatures of internal waves. The sea level anomalies in the study by Delcroix et al. 1991 were 10–15 cm. Such strong anomalies can be associated with the passage of internal waves with amplitudes of some tens of meters.

The above data suggest that the typical nonlinearity (defined as the ratio of the wave amplitude to the thermocline depth or, alternatively, as the ratio of the phase speed correction to the linear phase speed) may range from about 10% to 30%. For weaker waves, the nonlinearity may increase several-fold due to the shoaling of the thermocline (Long and Chang 1990; Yang and Yu 1992), as it decreases from 180 to 40 m, and sometimes even to 20 m, going from west to east.

One might assume that the phase speed corrections can be attributed to the mean currents, and especially to the effect of the equatorial undercurrent. However, calculations by Johnson and McPhaden (1993) for linear Kelvin waves show that adding the mean currents corrects the phase speed by only 4%. Thus there is sufficient evidence that nonlinearity may be important for equatorial Kelvin waves.

Since Kelvin waves are observed in the Pacific as well as the Atlantic Ocean (Katz 1987), the present work is applicable for both basins. However, as the Pacific basin is of greater size, the waves there have longer time for nonlinear evolution. The zonal extent of the Pacific in the equatorial region is approximately 145°, or about 16 000 km. In the next sections we will show that this may give the wave enough time to break and evolve into a fully developed front. Our results may be applicable also to the atmosphere where equatorially trapped Kelvin waves are well documented. For a review see Gill (1982).

Solving the full nonlinear shallow-water equations numerically we demonstrate that the wave steepens and approaches breaking in a manner qualitatively similar to that discussed by Boyd (1980) and Ripa (1982). However, after breaking and some adjustment, the Kelvin front[1] is formed with properties rather different from classical two-dimensional hydraulic jumps. Note that both Boyd and Ripa assumed geostrophic balance for the zonal component of the velocity. This assumption renders the nonlinear Kelvin waves straight-crested. Further, it permits the reduction of the problem of the wave evolution to a two-dimensional problem (with one spatial coordinate along the equator, and time). Thus,

---

[1] Sometimes any nonlinear Kelvin wave is referred to as a Kelvin wave front. We choose to use the word front in the narrower sense: a wave led by a hydraulic jump or shock.

wave breaking and fronts in their formulations are essentially two-dimensional.

In our work we show that, although the geostrophic balance holds during the initial stages of the wave evolution, a full three-dimensional model is needed to describe the developed front. In such a model, the temporal derivative of the transverse or meridional velocity is retained in the y-momentum equation, permitting curved fronts.

The Kelvin front is convex to the east with the equator as the axis of symmetry. A packet of gravity–inertial (or Poincaré) waves is generated, which travels at the same speed as the front. Although the cross-equatorial flow measured at the equator remains zero, the propagation of a Kelvin front leads to a nonzero net mass transport that is directed away from the equator above the thermocline. The maximum of this transport occurs at approximately one Rossby radius off the equator.

We explain these and other properties of Kelvin fronts within a semianalytical theory based on jump conditions and the approximation of a gravity–inertial boundary layer behind the jump. (For instance, the asymptotic angle of the front is given by a simple function of the front amplitude.) The major differences between the numerics and the theory is that in the latter we postulate the existence of the jump, and, thereby, obtain the wave field behind the front, while in the former the jump emerges after the evolution of the originally smooth initial disturbance.

Finally, by introducing a sloping thermocline and moderate asymmetry into the problem, we demonstrate that the formation of the Kelvin front is a robust feature of the model. (Although Long and Chang 1990 and Yang and Yu 1992 have considered the propagation of Kelvin waves on a slowly varying thermocline, neither of the studies dealt with front formation.)

2. Formulation of the problem

Internal waves trapped on the equatorial thermocline can be described by nonlinear shallow-water equations for a single-layer fluid on the equatorial beta plane lying on a deep motionless layer (the 1½-layer approximation):

$$u_t + uu_x + vu_y + g^*h_x - fv = 0, \quad (2.1)$$

$$v_t + uv_x + vv_y + g^*h_y + fu = 0, \quad (2.2)$$

$$h_t + (uh)_x + (vh)_y = 0, \quad (2.3)$$

where

$$f = \beta y. \quad (2.4)$$

The notation is conventional (Pedlosky 1987, p. 61), with positive $h(x, y, t)$ denoting the entire local depth of the thermocline, $u(x, y, t)$ the eastward velocity component, $v(x, y, t)$ the cross-equatorial (transverse) velocity, and g^* the effective (reduced) gravity. Note that

rearward breaking is not allowed in such a single-layer model unless we change the signs of the nonlinear terms. Nor do mean currents enter the equations, although their potential influence is briefly discussed in the introduction and in the discussion of section 4.

Following the standard approach, we introduce nondimensional variables

$$u = \alpha c u', \quad (2.5)$$

$$v = \alpha c v', \quad (2.6)$$

$$h = Dh', \quad \text{and} \quad (2.7)$$

$$x = \text{Ro}x', \quad (2.8)$$

$$y = \text{Ro}y', \quad (2.9)$$

$$t = \frac{\text{Ro}}{c}t', \quad (2.10)$$

where

$$\alpha = a/D, \quad (2.11)$$

$$c = \sqrt{g^*D}, \quad \text{and} \quad (2.12)$$

$$\text{Ro} = \sqrt{c/\beta}. \quad (2.13)$$

Here a is the characteristic wave amplitude, D is the undisturbed depth of the thermocline, c is the linear phase speed of internal gravity waves, and Ro is the (internal) equatorial Rossby radius of deformation. (For typical equatorial conditions Ro is approximately 300 km.)

Substituting (2.4)–(2.13) into (2.1)–(2.3) and dropping the primes gives the nondimensionalized shallow-water equations

$$u_t + \alpha(uu_x + vu_y) + h_x - yv = 0, \quad (2.14)$$

$$v_t + \alpha(uv_x + vv_y) + h_y + yu = 0, \quad (2.15)$$

$$h_t + \alpha(uh)_x + \alpha(vh)_y = 0, \quad (2.16)$$

where

$$h = 1 + \alpha\eta, \quad (2.17)$$

and η is the dimensionless displacement of the thermocline. Note that, unlike Boyd (1980) and Ripa (1982), we do not use the geostrophic approximation in the y-momentum equation (2.15) allowing for the possibility of curved fronts. In the flux-conserving form, the equations become

$$(uh)_t + \left(\alpha u^2 h + \frac{h^2}{2}\right)_x + \alpha(uvh)_y - yvh = 0, \quad (2.18)$$

$$(vh)_t + \alpha(uvh)_x + \left(\alpha v^2 h + \frac{h^2}{2}\right)_y + yuh = 0, \quad (2.19)$$

$$h_t + \alpha(uh)_x + \alpha(vh)_y = 0 \quad (2.20)$$

[cf. the f-plane case: Pratt (1983, 1987)]. The system (2.18)–(2.20) can account for classical hydraulic jumps

(Lighthill 1978; Whitham 1980) with rotation [see Fedorov and Melville (1996); Kuo and Polvani (1997); and Helfrich et al. (1999) for the f-plane case], that is, discontinuities in the wave field, with mass and momentum fluxes conserved across the jumps.

To describe physical fronts with a finite width and an internal structure, we add eddy viscosity ν in a way that is common to other tropical and equatorial problems (Gent 1993):

$$(uh)_t + \left(\alpha u^2 h + \frac{h^2}{2}\right)_x + \alpha(uvh)_y - yvh$$

$$= \nu((hu_x)_x + (hu_y)_y), \qquad (2.21)$$

$$(vh)_t + \alpha(uvh)_x + \left(\alpha v^2 h + \frac{h^2}{2}\right)_y + yuh$$

$$= \nu((hv_x)_x + (hv_y)_y) \qquad (2.22)$$

$$h_t + \alpha(uh)_x + \alpha(vh)_y = 0 \qquad (2.23)$$

In this latter system, the fronts appear as regions with large gradients of the relevant parameters (u, v, and h). We will use both systems (2.14)–(2.17) and (2.21)–(2.23) to analyze the evolution of equatorial Kelvin waves and development of the Kelvin fronts.

We have also completed several numerical runs using a different form of the mixing terms, namely

$$\nu[(uh)_{xx} + (uh)_{yy}] \quad \text{and} \quad \nu[(vh)_{xx} + (vh)_{yy}]. \quad (2.24)$$

The results were almost identical for different mixing parameterizations, as long as the eddy viscosity is small. The use of (2.24) is more convenient for numerical purposes, although not as general as the use of conventional mixing terms in (2.21)–(2.23).

The initial conditions for Eqs. (2.21)–(2.23) are chosen to correspond to a linear bell-shaped Kelvin wave stretched in the direction of the equator:

$$h|_{t=0} = 1 + \alpha \exp\left(-\frac{y^2}{2} - \frac{x^2}{2q^2}\right), \qquad (2.25)$$

$$u|_{t=0} = \alpha \exp\left(-\frac{y^2}{2} - \frac{x^2}{2q^2}\right), \qquad (2.26)$$

$$v|_{t=0} = 0, \qquad (2.27)$$

where q is the aspect ratio of the equatorial length of the disturbance to its width. It is usually assumed that for the equatorial Kelvin waves q is larger than unity. Further, in section 4 we will investigate the effect of a moderate displacement of such initial disturbance away from the equator.

For initial conditions (2.25)–(2.27) we could use the (slightly modified) result due to Boyd (1980) and Ripa (1982) to estimate the nondimensional time to breaking:

$$t_{\text{breaking}} \approx \frac{q}{\alpha}(2e/3)^{1/2}. \qquad (2.28)$$

For example in our calculations, we will take $D = 100$ m and $g^* = 0.05$ m s^{-2}, while $q \approx 3$ and $\alpha = 0.2$, yielding $c = 2.2$ m s^{-1} Ro $= 320$ km and $a = 20$ m, and $t_{\text{breaking}} \approx 18$. The full length of the disturbance given in (2.25)–(2.27) is about 20Ro (see Fig. 2a), corresponding to a wave period of approximately 33 days. Such a wave would break at $t_{\text{breaking}} \approx 18$ or, in dimensional units, after about one month of evolution. Before breaking, the wave would travel a distance of the order of 7000 km, significantly less than the width of the Pacific. Although in this particular example the wave amplitude is relatively high, less stretched disturbances of proportionately smaller amplitude would require the same time to break. As long as the wave is broken, it may form a Kelvin front.

Note that the typical breaking commonly associated with wave overturning never happens in our model since we have added eddy viscosity into the system. Instead, strong velocity gradients emerge in front of the wave. In the field this would lead to strong mixing and turbulence in the transitional region. We still refer to this phenomenon as wave breaking.

3. Nonlinear evolution of equatorial Kelvin waves and the formation of a Kelvin front

Now we numerically solve the shallow-water equation with friction (2.21)–(2.27). We use a scheme similar to that of MacCormac [an explicit scheme of the predictor–corrector type: see Fletcher (1991)]. The difference is that the nonlinear advective terms in (2.21)–(2.23) are given by centered finite differences. The scheme has second-order accuracy in both space and time. The coefficient of eddy viscosity ν, the longitudinal resolution of the grid Δx, and latitudinal resolution Δy are chosen to be linearly related to each other so that

$$\nu = A\Delta x, \qquad \Delta t = B\Delta x, \quad \text{and} \quad \Delta y = C\Delta x, \quad (3.1)$$

where A, B, and C are numerical coefficients. With better resolution (smaller Δx), the viscosity decreases. We introduce A, B, and C to meet several objectives. First, varying A and Δx we achieve the values of eddy viscosity conventionally accepted for these types of oceanic motion. Second, by varying the coefficients we change the properties of the scheme associated with front properties. Thus, we can have dissipative rather than dispersive jumps. (The former dissipates the energy in the jump itself through turbulence, while the latter looses energy by radiating waves that travel away from the jump; e.g., Whitham 1974). Finally, changing A, B, and C, we optimize the convergence of the scheme.

For the numerical runs presented in this section we take $\Delta x = 0.008$, and $A = 0.17$, $B = 0.34$, and $C = 0.58$. Other choices of A, B, and C are possible, but these were found to be optimal within the range of parameters considered. This particular choice of A and Δx gives $\nu = 0.0014$, which corresponds to a dimensional
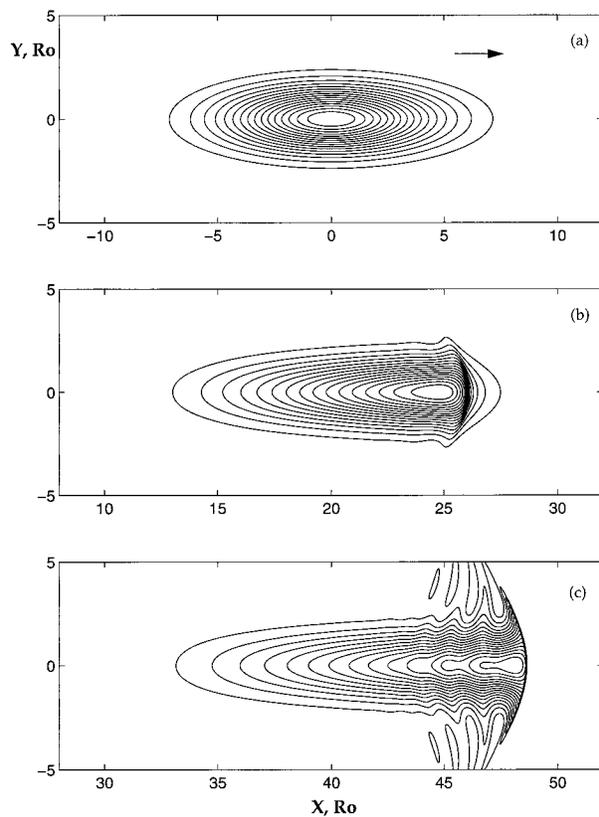
FIG. 2. The formation of a Kelvin front on a uniform thermocline from an initial disturbance corresponding to a linear Kelvin wave, which is Gaussian-shaped and stretched along the equator. The isolines of the displacement of the thermocline $\alpha\eta$ are shown. The depression of the thermocline is calculated by solving an initial value problem for the full shallow-water Equations (2.21)–(2.23) and initial conditions (2.25)–(2.27). The plots describe an approximately two-month period during the evolution of the wave ($\alpha = 0.2$ and $\nu = 0.0014$) (a) $t = 0$, (b) $t = 20$, and (c) $t = 40$.

value of the horizontal eddy diffusion of 10^3 m^2 s^{-1} if we use $c = 2.2$ m s^{-1} for the linear phase speed of Kelvin waves. Increasing Δx, while fixing A, B, and C, changes the solutions only slightly, amplifying viscosity and widening the region associated with the hydraulic jump. For further details of the numerics see Fedorov and Melville (1996).

In Fig. 2 we present an example of Kelvin wave evolution. Starting from its initial Gaussian shape, the equatorially trapped disturbance steepens, which is revealed in the higher concentration of contour lines on the front (Figs. 2a,b). The wave approaches breaking, and a curved front begins to form (Fig. 2b). Finally, the wave evolves into a fully developed Kelvin front (Fig. 2c). The front is convex to the east, and a complex crest pattern has emerged behind it. In the next section we will show that this pattern consists of Poincaré waves.

Figure 3 presents the amplitude of the wave as a function of time. The amplitude is defined as the maximum displacement of the thermocline on the equator. Although the values of the amplitude vary only slightly,
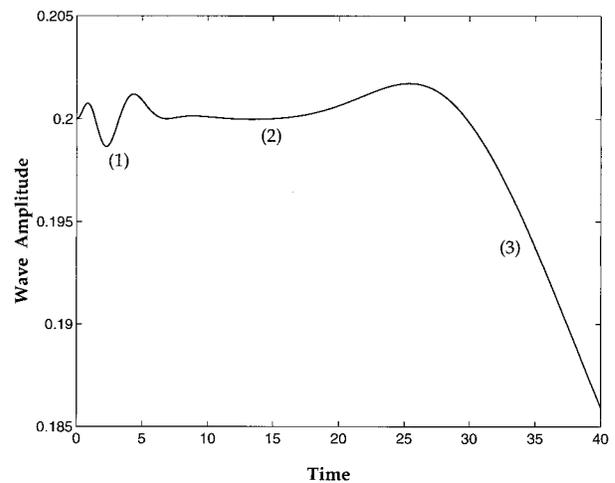

FIG. 3. The nondimensional amplitude of the wave (defined as the maximum displacement of the thermocline scaled by its depth) as a function of time for the wave evolution presented in Fig. 2. The oscillatory part of the graph (1) corresponds to the initial nonlinear adjustment and the excitation of a Rossby wave. The middle part of the graph (2) describes wave steepening leading to breaking. The relatively steep slope on the right (3) follows the formation of a Kelvin front, which strongly enhances dissipation.

one can distinguish several important regions of the graph. Clear oscillations of the amplitude on the left-hand side of the plot are related to the initial nonlinear adjustment of the wave. Since our initial conditions (2.25)–(2.27) are not an exact solution of the shallow-water equations, a relatively weak Rossby wave must emerge and travel westward, carrying excess energy. [This is analogous to the linear problem: see Gill (1982), Philander (1981), and Philander et al. (1984).] The region where the amplitude varies very little corresponds to wave steepening close to breaking. The right-hand side of the graph, with a relatively steep slope, is related to the formation of a Kelvin front. As soon as the front is developed, it causes a higher dissipation rate of the wave field.

4. Resonant generation of Poincaré waves

The detailed structure of the front and the wave field behind it is shown in Fig. 4, while the structure of the transverse (cross-equatorial) velocity field is given in Fig. 5. One of the most striking features of the wave development of the front (Figs. 2c, 4, and 5) is the appearance of relatively short waves behind it. Identification of these waves is facilitated by considering their cross-equatorial velocity field since the typical asymmetric cell structure in Fig. 5 can correspond only to the first Poincaré (gravity–inertial) mode. The group speed of the very short Rossby waves is too small to keep pace with a fast Kelvin wave (Fig. 6), while the higher Poincaré modes would have more nodes in the y direction. The remaining Yanai (mixed Rossby–grav-
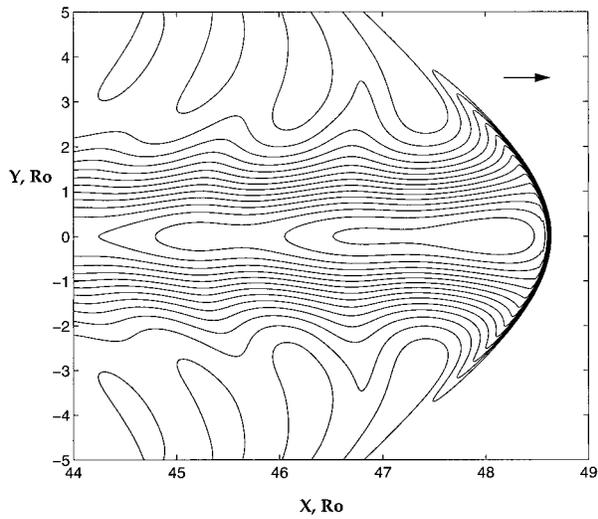
FIG. 4. The detailed structure of the Kelvin front and the wave field behind it (a blowup of Fig. 2c). The depression of the thermocline is shown. Notice the forced Poincaré (or trapped gravity–inertial) waves and the characteristic curved shape of the Kelvin front. The wavelength of Poincaré waves is determined by the speed of the front (or its amplitude) and can be calculated from the resonant condition (section 4).
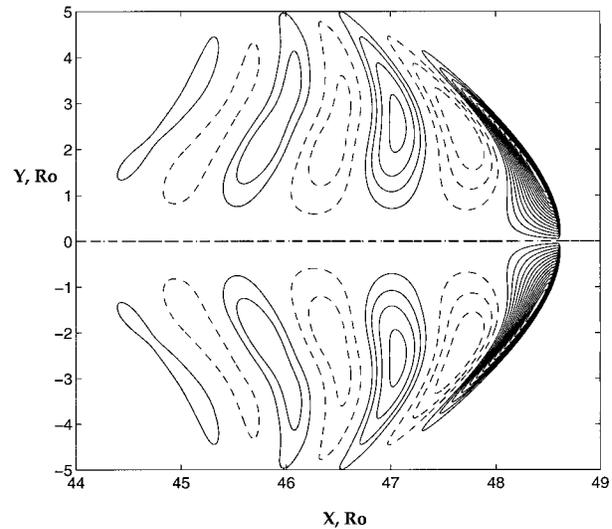

FIG. 5. Details of the transverse velocity field behind the jump. Isolines of the y component of the velocity v are shown. Note that solid (dashed) contours correspond to the flow directed away from (toward) the equator. There is no flow across the equator (at $y = 0$). The concentration of the isolines behind the jump is associated with the frontal off-equatorial jet caused by large gradients of the longitudinal velocity component. Notice the cell structure of Poincaré waves (see section 4).

ity) wave would have a nonzero transverse velocity at the equator.

The Poincaré waves are forced by the Kelvin front as a result of a direct resonance: The front is supercritical and moves slightly faster than a linear Kelvin wave so that it matches the phase speed of the Poincaré waves of an appropriate frequency (or wavelength) as shown in Fig. 6. This is similar to the case considered by Melville et al. (1989) and Tomasson and Melville (1992) in which a nonlinear coastal Kelvin wave gen-

erated secondary Poincaré waves in a strait. We emphasize, however, that in Melville et al. the Poincaré wave generation was a time-dependent process, leading the continual excitation of Poincaré waves and to decay of the Kelvin wave. In the present study the Poincaré wave pattern is attached to the front, travels with the same speed as the front, and remains almost steady with respect to the front after some initial development. This
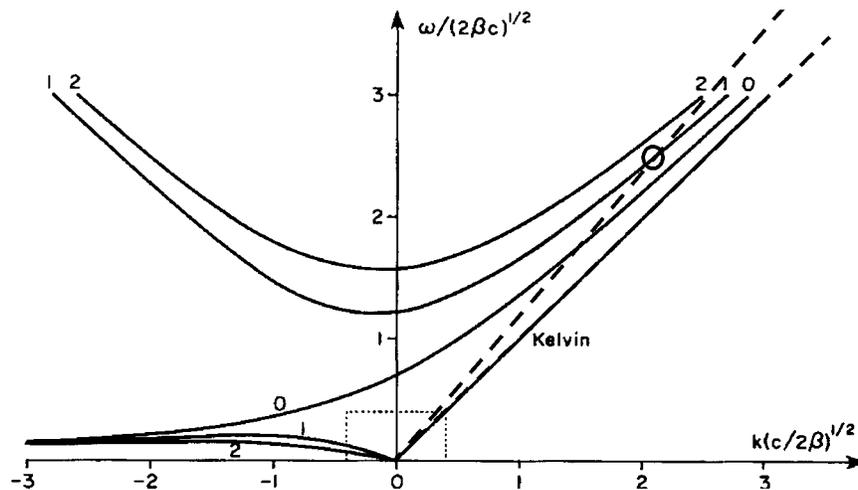

FIG. 6. Dispersion curves for equatorial waves. The curve labeled 0 corresponds to the mixed Rossby–gravity wave, the curves labeled 1 and 2 correspond to the first two gravity–inertial (or Poincaré) wave modes (from Gill 1982). The circle indicates the resonant condition for the generation of Poincaré waves by a nonlinear Kelvin wave.

will be used in section 6 in constructing a semianalytic theory of steady equatorial Kelvin fronts.

Nevertheless, in the initial value problem the Kelvin front is only quasi-steady since in a finite time the effect of the jump can be felt only at a finite distance away from it. The Poincaré waves are slowly spreading behind the front, which can happen because the group velocity of Poincaré waves is slightly smaller than that of a nonlinear Kelvin wave (Fig. 6).

To check the validity of the resonant mechanism we can estimate the wavelength λ_p of the Poincaré waves seen in Fig. 4. From Gill (1982) the frequency of the first Poincaré mode satisfies the nondimensionalized dispersion relation,

$$\omega^2 - k^2 - \frac{k}{\omega} = 3, \qquad (4.1)$$

where $k = 2\pi/\lambda_p$ is the wavenumber (shown in Fig. 6). Equation (4.1) can be rewritten, using the nondimensional phase speed $c_p = \omega/k$ of the Poincaré waves as

$$k^2 = \frac{3 + 1/c_p}{c_p^2 - 1}. \qquad (4.2)$$

If resonance occurs, the phase speed in (4.2) coincides with the speed of the front; that is,

$$c_p^2 = \left(1 + \frac{\Delta c}{c}\right)^2 \approx 1 + 2\frac{\Delta c}{c}, \qquad (4.3)$$

where $\Delta c/c$ is the nondimensional nonlinear correction to the phase speed of the linear Kelvin wave. Making use of (4.3) in (4.2) yields

$$k^2 \approx \frac{2c}{\Delta c}, \quad \text{or} \qquad (4.4)$$

$$\lambda_p \approx \pi\sqrt{2\frac{\Delta c}{c}}. \qquad (4.5)$$

We estimated $\Delta c/c$ from our numerical solution (presented in Figs. 3–5) to be about 0.13 by the time the front is formed. Substituting this value in (4.5) gives $\lambda_p \approx 1.6$, which agrees well with the figures.

The resonant approach gives some insight into the possible influence of the mean currents. Their main effect will be to modify the resonant condition locally. This would result in a change in the wave field, which may possibly alter the local shape of the jump (see section 6). However, the qualitative behavior and properties of the Kelvin front should not change.

5. Formation of Kelvin fronts: Sloping thermocline and asymmetry

To show that the formation of the Kelvin fronts is a robust feature of the model ocean in this parameter range, we pursue two additional numerical experiments. In the first experiment, we introduce a sloping ther-

mocline instead of the flat thermocline. While keeping the initial conditions and momentum equations as in the section 2 we change the continuity equation (2.23) to

$$h_t + \alpha\{u[h + \gamma(x - x_0)]\}_x + \alpha\{v[h + \gamma(x - x_0)]\}_y$$

$$= 0, \qquad (5.1)$$

where the extra term $\gamma(x - x_0)$ describes the effect of a shoaling thermocline with a constant slope γ and centered at $x = x_0$, which is approximately the half-width of the Pacific (about 30Ro). The typical value of γ is 0.02. For a single-layer ocean the additional term $\gamma(x - x_0)$ is equivalent to the introduction of sloping topography (Pedlosky 1987; Long and Chang 1990). With this change one can easily rewrite Eqs. (2.21) and (2.22) as

$$(uH)_t + \left(\alpha u^2 H + \frac{H^2}{2}\right)_x + \alpha(uvH)_y - yvH - \gamma H$$

$$= \nu((Hu_x)_x + (Hu_y)_y) \qquad (5.2)$$

$$(vH)_t + \alpha(uvH)_x + \left(\alpha v^2 H + \frac{H^2}{2}\right)_y + yuH$$

$$= \nu((Hv_x)_x + (Hv_y)_y) \qquad (5.3)$$

$$H_t + \alpha(uH)_x + \alpha(vH)_y = 0, \qquad (5.4)$$

where

$$H = h + \gamma(x - x_0) \qquad (5.5)$$

is the full local depth of the thermocline. Note that

$$d(x) = 1 + \gamma(x - x_0) \qquad (5.6)$$

is the undisturbed depth of the thermocline, while Eqs. (5.2)–(5.4) are still written in the flux-conserving form, with the extra term $-\gamma H$ due to the linearly varying depth of the thermocline.

These equations are solved numerically as in the previous case. Figure 7 shows the evolution of the initial disturbance advancing on the sloping thermocline. The concentration of the isolines in the frontal part of the wave is now due to two factors: the reduction of the local speed of the wave because of the decreasing depth of the thermocline and, second, the effect of nonlinearity itself. Both factors work to cause the wave to break. Figure 8 gives the evolution of the absolute wave amplitude that grows until the wave is broken and the front is formed. There are three distinct regions of behavior, as in the previous case (cf. Fig. 3). However, the initial relative amplitude is now smaller, as compared to the case of the flat thermocline, but still sufficient for the front to form. (The initial relative amplitude, defined as the ratio of the wave amplitude to the local depth of the thermocline, is now about 0.15.)

As we mentioned already, the propagation of the Kelvin waves on a slowly varying thermocline has been
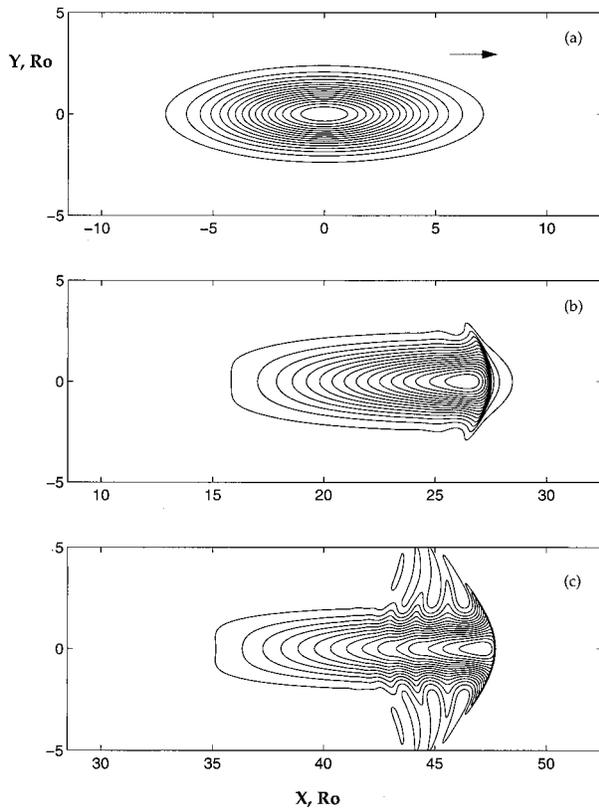
FIG. 7. The formation of a Kelvin front from an initial disturbance corresponding to a linear Kelvin wave on a thermocline of decreasing depth. The isolines of the displacement of the thermocline $\alpha\eta$ are shown. The depression of the thermocline is calculated by solving an initial value problem for the full shallow-water equation (5.2)–(5.4) with initial conditions (2.25)–(2.27). Here, $\alpha = 0.2$, $\nu = 0.0014$, and the thermocline has a slope $\gamma = 0.02$. The depth of the thermocline varies from about 150 to 50 m. The wave slows down during its eastward propagation because of the decreasing phase speed in the shallower thermocline: (a) $t = 0$, (b) $t = 20$, and (c) $t = 40$.

studied before. Yang and Yu (1992) used a linear model and apply the WKBJ method to obtain their solution. Long and Chang (1990) derived a KdV–type equation with varying coefficients for describing nonlinear Kelvin waves. Neither of the studies dealt with the fronts (hydraulic jumps). Importantly, in all previous studies it has been assumed that all different types of the equatorial waves become well separated after some time due to the differences in the phase speeds. As we have shown, it is not the case for the Kelvin jump for which Poincaré waves and the Kelvin wave do not separate. This is similar to the nonlinear Rossby adjustment in a channel (Tomasson and Melville 1992). The characteristic time scale of the nonlinear evolution is comparable to the time needed for the wave separation, in consequence of which full separation does not occur.

In the next example we introduce a mild asymmetry into the problem. To maintain consistency with the real ocean we retain the slope of the thermocline, but employ asymmetric initial conditions:
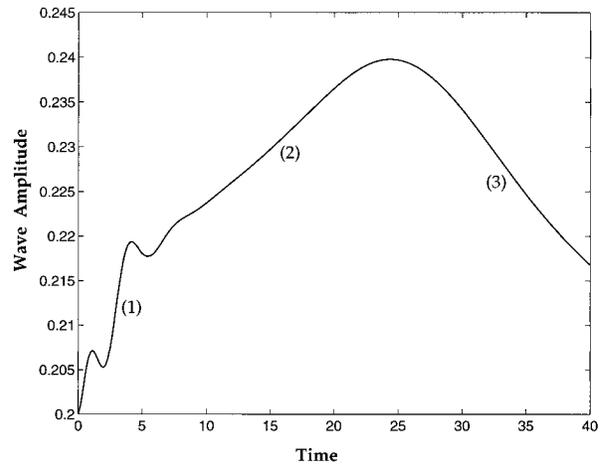

FIG. 8. The nondimensional amplitude of the wave (defined as the maximum displacement of the thermocline scaled by its mean depth) as a function of time for the wave evolution in Fig. 7. The oscillatory part of the graph (1) corresponds to the initial nonlinear adjustment and the excitation of a Rossby wave. The middle part of the graph (2) describes wave steepening leading to breaking. The increase in the amplitude is associated with the decreasing thermocline depth. The steep decay on the right (3) follows the formation of a Kelvin front, enhancing dissipation. Note that the relative amplitude of the wave, defined as the ratio of the maximum displacement of the thermocline to its local depth, increases from 0.15 to 0.45 during the propagation interval.

$$h|_{t=0} = 1 + \alpha \exp\left(-\frac{(y - \Delta)^2}{2} - \frac{x^2}{2q^2}\right), \quad (5.7)$$

$$u|_{t=0} = \alpha \exp\left(-\frac{(y - \Delta)^2}{2} - \frac{x^2}{2q^2}\right), \quad (5.8)$$

where Δ is the meridional shift of the initial disturbance with respect to the equator. For our calculations we chose it to be 0.5Ro. Although initial conditions (5.7)–(5.8) do not correspond to a pure Kelvin wave, they simulate an asymmetry in the near-equatorial processes due to various factors, for example, the effects of southerly winds.

There is only one major difference in the solutions compared to the previous cases. An asymmetric Yanai wave emerges from the initial disturbance and follows the Kelvin front at a slower speed (Fig. 9). After some time, the front and Yanai wave become completely separated. After the separation the front remains symmetric and does not differ from the previous cases (Fig. 9c).

6. Three-dimensional fine structure of Kelvin fronts

From the previous examples, we conclude that for a range of the initial conditions and thermocline structure an equatorial disturbance evolves into a Kelvin front, provided the disturbance has a sufficient amplitude. The front propagates with little change in shape or speed. It is possible to construct a semi-analytical theory for such
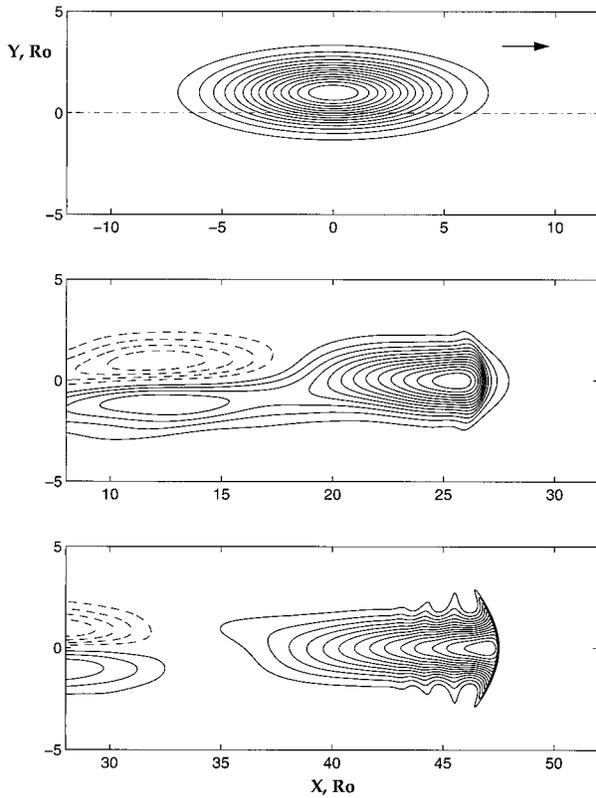
FIG. 9. The formation of a Kelvin front from an asymmetric initial disturbance corresponding to a linear Kelvin wave shifted northward with respect to the equator. The isolines of the displacement of the thermocline $\alpha\eta$ are shown. The depression of the thermocline is calculated by solving an initial value problem for the full shallow-water equations (5.2)–(5.4) with initial conditions (5.7)–(5.8). Here $\alpha = 0.2$, $\nu = 0.0014$, the thermocline shoals with the slope $\gamma = 0.02$, and the initial disturbance is shifted by $\Delta = 0.5$ northward with respect to the equator. Notice an antisymmetric Yanai wave emerging from the disturbance that follows the Kelvin front. After a little time the front and the Yanai wave become separated: (a) $t = 0$, (b) $t = 20$, and (c) $t = 40$.

a steady front, based on the classical hydraulic theory and a boundary layer approach. In this model the hydraulic jump is moving eastward with a constant speed and is trailed by a wave wake. Mass and momentum are conserved across the jump, which has negligible width. The analysis below closely follows the derivations for the case of coastal hydraulic jumps with rotation (Fedorov and Melville 1996) and is given here only briefly.

We take the inviscid shallow-water equations (2.14)–(2.17) and their flux-conserving counterparts (2.18)–(2.20) as the basis for our analysis. We transform to a frame of reference travelling eastward with the front. The speed of the front is $1 + s$, where $s = \Delta c/c = O(\alpha)$. That is, the speed of the jump is the phase speed of a linear Kelvin wave plus a nonlinear fractional correction s.

We assume that variables η, u, and v have a discontinuity of finite amplitude at the jump, which occurs

along a line $x = r(y)$ separating two regions in which the variables are continuous. The function $r(y)$ then determines the shape of the jump. For simplicity, we assume that there is no motion towards the jump from the east; that is, η, u, and v are zero for $x > r(y)$. Finally, we impose an additional constraint on the scales of the terms setting

$$v = O(\alpha^{1/2}), \tag{6.1}$$

which means that the off-equatorial flow is relatively weak. The small parameter in the following expansion will be $\alpha^{1/2}$.

Integrating Eqs. (2.18)–(2.20) with respect to x from $r - \varepsilon$ to $r + \varepsilon$, taking the limit as ε goes to zero, and neglecting higher order terms with respect to α gives us three jump conditions connecting the jump amplitudes in η, u, and v and $r(y)$:

$$\eta_\circ - u_\circ = su_\circ - \frac{\alpha}{2}u_\circ^2, \tag{6.2}$$

$$v_\circ = -r_y\eta_\circ, \tag{6.3}$$

$$u_\circ - \eta_\circ = s\eta_\circ + r_y v_\circ - \alpha u_\circ \eta_\circ, \tag{6.4}$$

where $\eta_\circ$, $u_\circ$, and $v_\circ$ depend upon y and correspond to the wave field immediately behind the jump (e.g., $u_\circ = u_{|x=r-0}$). Equation (6.3) implies that the transverse velocity is nonzero if the jump is curved, and vice versa.

From (6.1)–(6.4) we find that $u_\circ = \eta_\circ + O(\alpha)$. Adding (6.2) and (6.4) with the use of (6.3) gives

$$(r_y)^2 = 2s - \frac{3}{2}\alpha\eta_\circ. \tag{6.5}$$

This is an equation describing the shape of the front.

For waves symmetrical with respect to the equator, v is zero at the equator (at $y = 0$), which implies that

$$r_y = 0 \quad \text{at } y = 0, \tag{6.6}$$

and thus

$$s = \frac{3}{4}\alpha\eta_\circ|_{y=0}. \tag{6.7}$$

Without loss of generality, we assume that $\eta_\circ = 1$ so that the nondimensional correction to the jump speed becomes

$$s = \frac{3\alpha}{4}. \tag{6.8}$$

Behind the front there should exist an inertial boundary layer with a balance between rotation and nonlinearity. The main role of the layer is to adjust the transverse velocity to zero away from the front. [The off-equatorial velocity near the front is nonzero because of the bending of the front, which follows from Eq. (6.3).] Earlier, we have accounted for the appearance of Poincaré waves through direct resonance. In principle, the resonant and the boundary layer approaches are equivalent since the
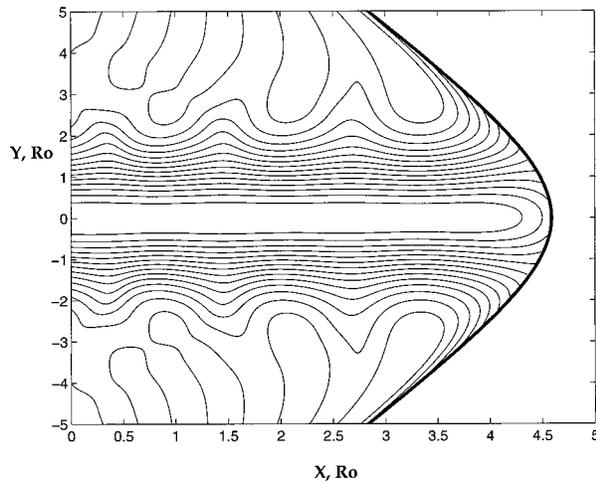
FIG. 10. The detailed structure of the Kelvin front and the wave field behind it from the approximate model of section 6 (cf. Fig. 4). The depression of thermocline is presented. The position of the jump is shown by the solid thick line. These results were obtained by solving the reduced shallow-water Equations (6.11)–(6.12) with the "jump" boundary conditions (6.13)–(6.16) for $\alpha = 0.185$ and a flat thermocline. Note the forced Poincaré waves.
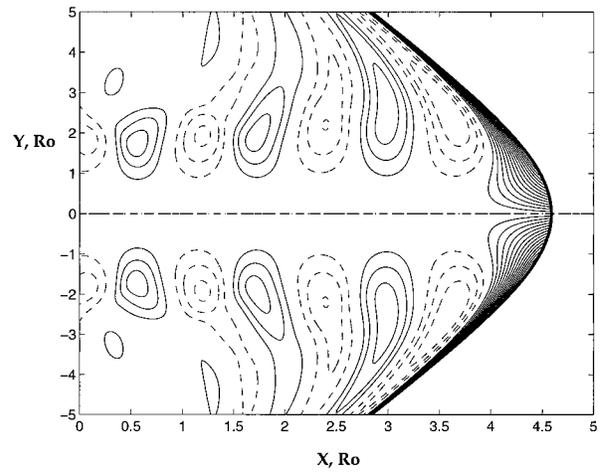

FIG. 11. The detailed structure of the transverse velocity field behind the Kelvin front from the approximate model of section 6 (cf. Fig. 4). (top view, cf. Fig. 5). The position of the jump is shown by the solid thick line. Note that solid (dashed) contours correspond to the flow directed away from (toward) the equator. There is no flow across the equator (at $y = 0$). These results are obtained by solving the reduced shallow-water equations (6.11)–(6.12) with the "jump" boundary conditions (6.13)–(6.16) for $\alpha = 0.185$ and a flat thermocline. Notice the cell-like structure of the forced Poincaré waves.

Poincaré waves are necessary to resolve the nonzero transverse velocity behind the front.

The scale analysis shows that the characteristic scale of the boundary layer correction in the x direction should be $O(\sqrt{\alpha})$ (see Fedorov and Melville 1996). Using this scaling, we return to the shallow-water equations (2.14)–(2.16) to find that for the eastward-propagating waves,

$$u = \eta + O(\alpha). \qquad (6.9)$$

Considering terms at the next order, we add Eqs. (2.14) and (2.16) to obtain for the steady-wave solutions

$$v_y - yv - su_x - s\eta_x + \alpha u u_x + \alpha(u\eta)_x = 0. \qquad (6.10)$$

Substituting (6.9) in (6.10) and in (2.15) and neglecting higher-order terms gives

$$v_y - yv = 2s\eta_x - 3\alpha\eta\eta_x, \qquad (6.11)$$

$$-v_x + \eta_y + y\eta = 0. \qquad (6.12)$$

This set now replaces the full shallow-water equations. We emphasize that the set of equations (6.11) and (6.12) expresses a balance between the effects of nonlinearity and rotation in the boundary layer behind the jump.

The boundary conditions for the system (6.11)–(6.12) should be defined at the equator (the no-flow condition), at the jump itself, and far away from the jump. The equation describing the shape of the front (6.5) then becomes the first boundary condition, while the jump condition (6.3) connecting $\eta_\circ$ and $v_\circ$ becomes the second boundary condition at the jump line. We also require that for large x the wave field structure in the y direction be Gaussian so that the unified boundary conditions become

$$v = 0 \qquad\qquad \text{at } y = 0, \qquad (6.13)$$

$$\frac{3}{2}\alpha\eta = 2s - (r_y)^2 \qquad \text{at } x = r(y), \qquad (6.14)$$

$$v = -r_y\eta \qquad\qquad \text{at } x = r(y), \qquad (6.15)$$

$$\eta \sim K \exp(-y^2/2) \quad \text{at } \hat{x} \to -\infty, \qquad (6.16)$$

where s is given by (6.8), and (6.16) ensures that the shape of the wave upstream is Gaussian. A constant K is introduced to allow for adjustment of the wave height away from the jump.[2] It is needed because we have already scaled the equations assuming that $\eta_\circ = 1$. As shown in the next section, mass transport considerations require that

$$K = \sqrt{\frac{3}{2}}. \qquad (6.17)$$

Thus, to find the wave field behind the jump and the shape of the jump, we need to solve Eqs. (6.11)–(6.12) with the boundary conditions (6.13)–(6.16). Although the equations are relatively complex and the boundary conditions are determined at an unknown boundary, the set brings much more insight to the structure of the jump and its characteristics. For example, we can determine the angle φ between the tangent to the jump for large y on each side of the equator and the meridian. Using (614) and (6.16) gives

---

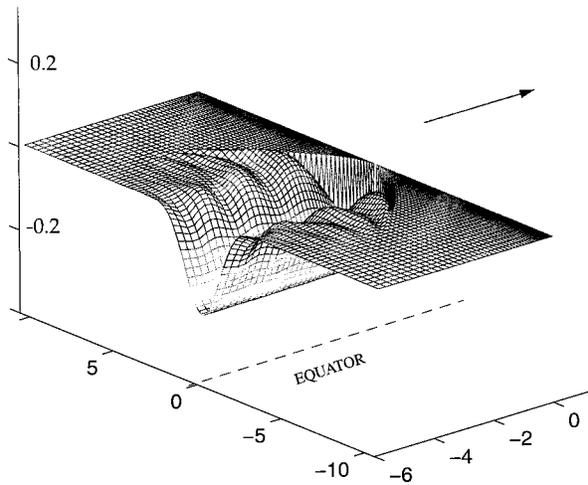[2] See Fedorov and Melville (1996) for a discussion.

FIG. 12. A perspective view of a Kelvin front steadily propagating eastward along the equator. The depression of thermocline behind a hydraulic jump is shown. The Poincaré waves are attached to the jump. The direction of propagation is indicated by the arrow ($\alpha = 0.185$).

$$r_y = -\sqrt{2s} \quad \text{at} \quad y \to -\infty, \qquad (6.18)$$

and for weak nonlinearity,

$$\varphi \approx \sqrt{2s} \quad \text{or} \quad \varphi \approx \sqrt{\frac{3}{2}\alpha}. \qquad (6.19)$$

We solve the system (6.11)–(6.17) numerically by introducing time-dependence in the equations and pursuing calculations until a steady limit is reached. The details of the numerical approach are analogous to those given in Fedorov and Melville (1996).

Figures 10 and 11 display a Kelvin front, the displacement of the thermocline, and the transverse velocity field behind the jump, which is obtained by solving Eqs. (6.11)–(6.16), while Fig. 12 shows a full view of the Kelvin jump. Note that there is a difference between the steady jump solution in this section and the solution of an initial value problem in section 3 since the latter is only quasi-steady and its wave field goes to zero for large x. In spite of this, the two solutions in Fig. 10 (11) and 4 (5) are very similar, especially in the vicinity of the jump.

Figures 13 and 14 show the displacement of the thermocline and the transverse velocity field as a function of x at different latitudes. There is a striking difference when compared with two-dimensional jumps. For instance, one can clearly see Poincaré waves, slowly decaying with x. Note that, since the wave field decays only slowly, the boundary layer extends far upstream and, in fact, becomes a lengthy boundary region behind the jump. In the boundary region, the characteristic scale $O(\sqrt{\alpha})$ is the scale of the undulations of the wave field, rather than its typical decay scale. This is a common feature of inertial boundary layers (Pedlosky 1987). The decay of the undulations is determined by energy leaking away from the equator, and friction if included.

Finally, Fig. 15 displays a cross section of the displacement of the thermocline along a meridian at some distance behind the most foremost point of the jump. There are overshoots caused by Poincaré waves at distances of 3.5Ro (approximately 1000 km) away from the equator, compared to a linear Kelvin wave solution. The overshoots are a result of the nonlinear dynamics. Delcroix et al. 1991 reported similar differences between the observed Kelvin waves and the linear theory
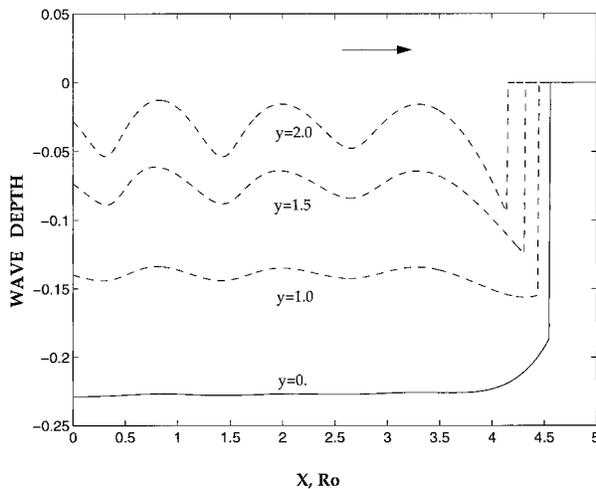

FIG. 13. The nondimensional depression of the thermocline ($-\alpha\eta$) following the jump at different distances away from the equator, that is, the cross sections of the wave field in Fig. 12 that are parallel to the equator. The jump and the undulations of the wave field due to Poincaré waves are clearly seen. Poincaré waves become significant at distances greater than one Rossby radius off the equator.
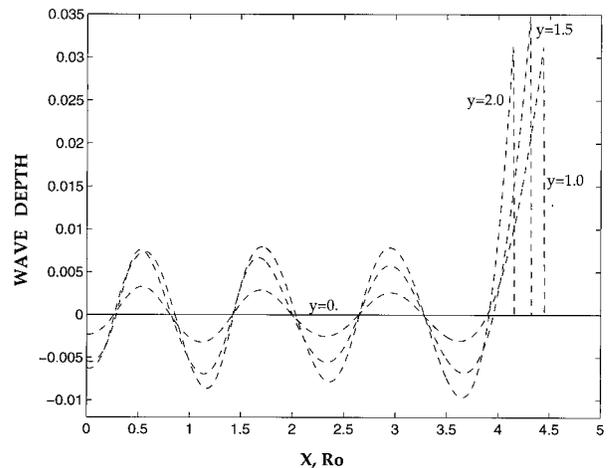

FIG. 14. The nondimensional transverse velocity field following the Kelvin jump at different distances away from the equator, that is, the cross sections of the velocity field that are parallel to the equator. The velocity is zero across the equator (at $y = 0$). There is a clear jump in the transverse velocity leading the pattern. As in Fig. 13, Poincaré waves become significant at distances greater than one Rossby radius.
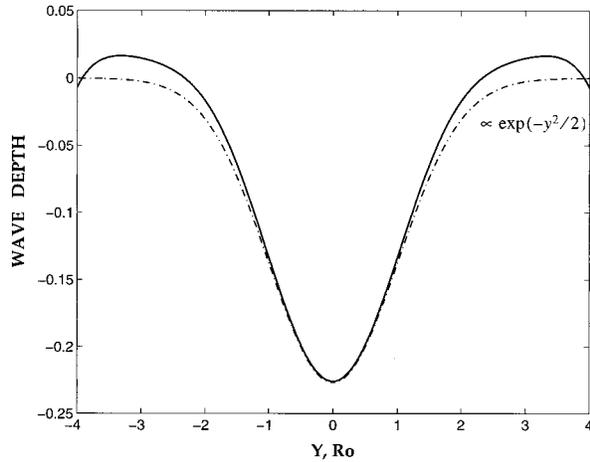
FIG. 15. The nondimensional displacement of the thermocline as a function of y at a distance of 1.35Ro along the equator behind the leading edge of the front (solid line). The background dashed line shows the corresponding Gaussian curve for a linear Kelvin wave. Notice the overshoots of the nonlinear wave at distances of approximately 3.5Ro away from the equator (cf. Delcroix et al. 1991).
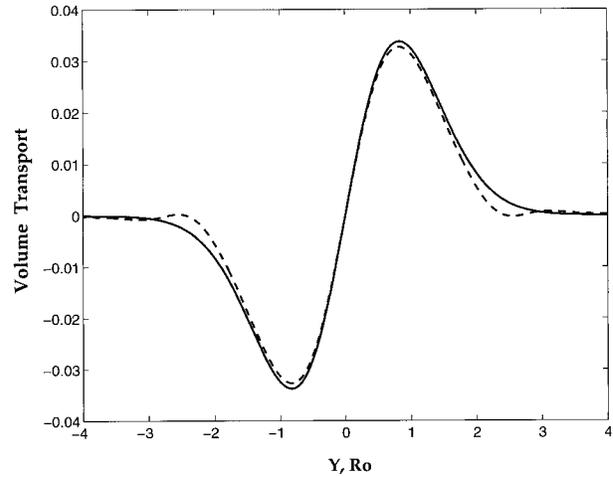

FIG. 16. The antisymmetric off-equatorial net volume transport as a function of y ($\alpha = 0.185$). The transport is maximum at distances O(Ro) away from the equator. The solid line is obtained by using formula (7.8). The dashed line corresponds to the numerically calculated transport, obtained by integrating the transverse velocity with respect to y. The differences are due to the finite resolution of the grid and the limited size of the basin in the numerical calculations.

occurring at the same distance, although the overshoots they detected were about two to three times as strong.

7. Off-equatorial mass transport

Using the formulations of the previous section we can calculate the net mass transport away form the equator as a function of y (or latitude). Introducing the volume transport T, where

$$T = T(y) = \int_{-\infty}^{r} v \, dx, \tag{7.1}$$

we integrate Eqs. (6.11) with the use of (6.14) and (6.15) to obtain

$$\frac{dT}{dy} - yT = 2s(\eta_\circ - Ke^{-y^2/2})$$

$$- \frac{3\alpha}{2}(\eta_\circ^2 - K^2 e^{-y^2}) + r_y v_\circ. \tag{7.2}$$

Further, using the boundary conditions (6.15) and (6.16) gives

$$\frac{dT}{dy} - yT = \frac{3\alpha}{2} K^2 e^{-y^2} - 2sKe^{-y^2/2}, \tag{7.3}$$

and after integration

$$T = \frac{\sqrt{\pi}}{2} e^{y^2/2} \left\{ 2sK \, \mathrm{erfc}(y) - \alpha K^2 \sqrt{\frac{3}{2}} \, \mathrm{erfc}\left(y\sqrt{\frac{3}{2}}\right) \right\}, \tag{7.4}$$

where $\mathrm{erfc}(z)$ is the complementary error function; that is,

$$\mathrm{erfc}(z) = \frac{2}{\sqrt{\pi}} \int_z^\infty e^{-w^2} \, dw. \tag{7.5}$$

Clearly,

$$T|_{y=0} = 0, \tag{7.6}$$

which requires that

$$K = \frac{2s}{\alpha}\sqrt{\frac{2}{3}} = \sqrt{\frac{3}{2}} \tag{7.7}$$

so that

$$T = \frac{3\alpha}{4}\sqrt{\frac{3\pi}{2}} e^{y^2/2} \left\{ \mathrm{erfc}(y) - \mathrm{erfc}\left(y\sqrt{\frac{3}{2}}\right) \right\}. \tag{7.8}$$

That is, the net meridional flow is nonzero and is proportional to the jump amplitude. The plot of $T(y)$ in Fig. 16 shows two extrema in the net off-equatorial transport at distances approximately equal to the Rossby radius. In these internal waves, any mass transport is associated with a heat flux. In the waves of depression we have considered, warmer water masses are replacing colder waters. This implies that the off-equatorial mass transport (as in the Fig. 16) leads a proportional positive heat flux directed away from the equator.

8. Conclusions

We have demonstrated the possibility of Kelvin fronts on the equatorial thermocline. Whether or not the fronts appear depends upon the wavelength and amplitude of the initial disturbance, as well as the width of the basin. The shoaling of the thermocline facilitates the formation

of the front. The front can emerge only from a wave of depression. Waves of elevation break on the rearward face, and are not considered here.

The properties of the Kelvin front derived from both the numerical model and semianalytical approach can be summarize as follows.

1) In the lee of the jump the wave field decays away from the equator in a quasi-Gaussian manner, which is similar to a regular Kelvin wave. Nevertheless, at some distance away from the jump there can be overshoots that distinguish the shape from pure Gaussian.

2) In the absence of dissipation the jump travels with a constant speed and maintains a permanent shape, which depends only on the jump strength. The dissipation and the limited extent of the initial conditions render the jump quasi-steady.

3) The jump curves back from the normal to the equator to straight oblique lines on each side of the equator. The angle included between these two lines and the meridian is a simple function of the jump amplitude at the equator.

4) As a result of resonant interactions Poincaré (i.e., trapped gravity–inertial) waves are generated behind the front and move with the same phase speed as the front. The resonance is possible because the speed of the front is slightly greater than that of a linear Kelvin wave. Together, the front and the Poincaré waves constitute a unified wave pattern. In contrast to the previous studies of the equatorial wave dynamics (e.g., Boyd 1980; Ripa 1982), in our model the nonlinear Kelvin and Poincaré waves do not separate.

5) Asymmetry of the initial conditions results in the generation of a Yanai (i.e., mixed Rossby–gravity) wave, which follows the front. However, after a short time the front and the Yanai wave become completely separated.

6) The Kelvin jump gives rise to a moderate net off-equatorial flow. Consequently, there is a contribution to the poleward heat flux. This feature is different from that of linear Kelvin waves, which have zero transverse flow.

There is indirect observational evidence that Kelvin fronts may exist. The amplitude of the observed Kelvin waves may be sufficient for the waves to break and for the fronts to emerge (e.g., Kessler et al. 1995). The observed meridional structure of the Kelvin waves is more complicated than a simple Gaussian distribution (Delcroix et al. 1991), analogous to the case considered here. There is some evidence of rapid temperature changes at the mooring sites of the TAO array (see, TAO Web site)[3] and in the TOPEX/Poseidon data (J. Picaut 1998, personal communication), which show that the wind-forced Kelvin waves, sometimes associated with the El Niño signal in the eastern Pacific, are clearly fronts rather than linear Kelvin waves. This may necessitate some corrections of the Kelvin wave speed and dissipation rates used in current models of the ENSO. Another important consequence of the study is that nonlinear Kelvin waves may be a source for gravity–inertial waves on the equatorial thermocline. Also, the effect of Kelvin fronts on the mixing processes should be considered.

Finally, Kelvin fronts may also exist in the equatorial regions of the atmosphere where they would be unimpeded by coastal boundaries. This is a subject for further study.

REFERENCES

Boyd, J. P., 1980: The nonlinear equatorial Kelvin wave. *J. Phys. Oceanogr.,* **10,** 1–11.

Delcroix, T., J. Picaut, and G. Eldin, 1991: Equatorial Kelvin and Rossby waves evidenced in the Pacific Ocean through Geosat sea level and surface current anomalies. *J. Geophys. Res.,* **96** (C10), 3249–3262.

Eriksen, C. C., M. B. Blumenthal, S. P. Hayes, and P. Ripa, 1983: Wind-generated equatorial Kelvin waves observed across the Pacific Ocean. *J. Phys. Oceanogr.,* **13,** 1622–1640.

Fedorov, A. V., 1997: Nonlinear effects in surface and internal waves. Ph.D. thesis. University of California, San Diego, 237 pp.

——, and W. K. Melville, 1995: On the propagation and breaking of nonlinear Kelvin waves. *J. Phys. Oceanogr.,* **25,** 2519–2531.

——, and ——, 1996: Hydraulic jumps at boundaries in rotating fluids. *J. Fluid Mech.,* **324,** 55–82.

Fletcher, C. A. J., 1991: *Computational Techniques for Fluid Dynamics.* Springer-Verlag, 480 pp.

Gent, P. R., 1993: The energetically consistent shallow-water equations. *J. Atmos. Sci.,* **50,** 1323–1325.

Gill, A. E., 1982: *Atmosphere–Ocean Dynamics.* Academic Press, 662 pp.

Helfrich, K., A. C. Kuo, and L. J. Pratt, 1999: Dam break in a rotating channel. *J. Fluid Mech.,* in press.

Johnson, E. S., and M. J. McPhaden, 1993: Structure of intraseasonal Kelvin waves in the equatorial Pacific Ocean. *J. Phys. Oceanogr.,* **23,** 608–625.

Katz, E. J., 1987: Equatorial Kelvin waves in the Atlantic. *J. Geophys. Res.,* **92** (C2), 1894–1898.

Kessler, W. S., M. J. McPhaden, and K. M. Weickmann, 1995: Forcing of intraseasonal Kelvin waves in the equatorial Pacific. *J. Geophys. Res.,* **100** (C10), 10 613–10 631.

Kuo, A. C., and L. M. Polvani, 1997: Time-dependent fully nonlinear geostrophic adjustment. *J. Phys. Oceanogr.,* **27,** 1614–1634.

Lighthill, M. J., 1978: *Waves in Fluids.* Cambridge University Press, 504 pp.

Long, B., and P. Chang, 1990: Propagation of an equatorial Kelvin wave in a varying thermocline. *J. Phys. Oceanogr.,* **20,** 1826–1841.

---

[3] Online at http://www.pmel.noaa.gov/toga-tao.

Melville, W. K., G. G. Tomasson, and D. P. Renouard, 1989: On the stability of Kelvin waves. *J. Fluid Mech.,* **206,** 1–23.

Pedlosky, J., 1987: *Geophysical Fluid Dynamics.* Springer-Verlag, 710 pp.

Philander, S. G. H., 1981: The response of equatorial oceans to a relaxation of the trade winds. *J. Phys. Oceanogr.,* **11,** 176–189.

——, 1990: *El Niño, La Niña, and the Southern Oscillation.* Academic Press, 293 pp.

——, T. Yamagata, and R. C. Pacanowski, 1984: Unstable air–sea interactions in the tropics. *J. Atmos. Sci.,* **41,** 604–613.

Pratt, L. J., 1983: On inertial flow over topography. Part 1. *J. Fluid Mech.,* **131,** 195–218.

——, 1987: Rotating shocks in a separated laboratory channel flow. *J. Phys. Oceanogr.,* **17,** 483–491.

Ripa, P., 1982: Nonlinear wave–wave interactions in a one-layer reduced-gravity model of the equatorial beta-plane. *J. Phys. Oceanogr.,* **12,** 97–111.

Tomasson, G. G., and W. K. Melville, 1992: Geostrophic adjustment in a channel: Nonlinear and dispersive effects. *J. Fluid Mech.,* **241,** 23–57.

Whitham, G. B., 1974: *Linear and Nonlinear Waves.* Wiley and Sons, 636 pp.

Yang, J., and L. Yu, 1992: Propagation of equatorially trapped waves on a sloping thermocline. *J. Phys. Oceanogr.,* **22,** 573–583.